Determination of the Network Structure of Sensor Materials Prepared by Three Different Sol-Gel Routes Using Fourier Transform Infrared Spectroscopy (FT-IR)

Larissa B. Cappeletti,[a] Edwin Moncada,[b] Joel Poisson,[c] Ian S. Butler,[c] João Henrique Z. Dos Santos[a,*]

[a] *Instituto de Química, UFRGS, Av. Bento Gonçalves, 9500, Porto Alegre, Brazil*
[b] *Instituto Tecnológico Metropolitano, Robledo, Calle 73, #76A-354, Bloque F, Medellín, Colombia*
[c] *Department of Chemistry, McGill University, 801 Sherbrooke Street, West, Montreal, Canada H3A 2K6*

Solid acid–base sensor materials were prepared by encapsulating three pH indicators (alizarin red, brilliant yellow, and acridine) within a silica matrix using a sol-gel approach through three different routes: (1) non-hydrolytic, (2) acid-catalyzed, and (3) base-catalyzed. Raman and Fourier transform infrared spectroscopies were used to evaluate the silica–indicator interactions. Because vibrational bands assigned to functional groups present in the indicator molecules were not detected, the main silica stretching mode ν_{Si-O} between approximately 1300 and 1000 cm^{-1} was used to detect the presence of our indicators within the silica matrix. The large band centered at 1100 cm^{-1} was deconvoluted into four components corresponding to the longitudinal optic and transversal optic modes of the silicon monoxide $(SiO)_4$ and $(SiO)_6$ siloxane rings. Using the component area of each mode, it was possible to calculate the percentage of each structure. Such percentages ranged from 49% to 70% $(SiO)_6$ for the analyzed samples, within a confidence level of 95% ($p = 0.05$). (The confidence limits were 53–62%.) These results could be related to the pH indicator content, indicating that the quantity of the encapsulated molecule affects the $(SiO)_6$ percentage values. In addition, a comparison with the radius of gyration obtained by small angle X-ray scattering was done. These results indicate that the analyte accesses the receptor elements through the passages between the siloxane rings but not through the siloxane rings themselves.

Index Headings: **Sensor material; Sol-gel process; Fourier transform infrared spectroscopy; FT-IR; Raman; Silica.**

INTRODUCTION

Interest in monitoring chemical and food industry processing, as well as environmental and health-related issues, has spurred the design of new sensors that are versatile, specific, robust, and sensitive.[1–4] One of the most common approaches to improve and design new sensors is the immobilization of receptor elements within a silica matrix by the sol-gel process, especially in the development of pH sensors through the encapsulation of pH indicators.[5–7] This improvement is due to the versatility of silica and beneficial material properties associated with the sensor morphology, such as optical transparency, mechanical stability, chemical roughness, and flexibility.[7–9] In addition, this type of matrix is permeable to analytes, while keeping the receptor element inside. This process also allows researchers to tune the matrix characteristics with respect to the final application.[5,10]

For the design of these matrix characteristics, a structural analysis of the materials is important because interactions between the encapsulated molecules and the matrix are critical for sensor performance. In a structural analysis, these encapsulated molecules can be investigated in terms of their interactions with the silica network and with respect to the function of the silica network itself. To this end, several techniques were used, such as ultraviolet (UV)-visible (vis) spectroscopy,[5,11,12], Fourier transform infrared (FT-IR) spectrometry,[13,14] X-ray photoelectron spectroscopy,[13,15] and cyclic voltammetry.[16,17]

Fourier transform infrared spectrometry was used to determine parameters of the silica network as a function of the hydrophilicity/hydrophobicity degree and the siloxane ring structure[14,18] with respect to thin film porosity.[19] In sensors, these characteristics influence the interaction and access the analyte has to the encapsulated molecule within the silica matrix. If the encapsulated molecules are interacting through their active sites, it is possible that these active sites are not available to further interact with the analyte. Poor sensor performance is also possible if the network is blocked. In this case, it is possible to hinder the reaction with the analyte. The silica network itself limits the pathways that the analyte can travel to reach the encapsulated receptor molecules. Subsequently, both cases could reduce the sensor performance or completely disable it. Other techniques have been used to determine structural changes as a result of the presence of foreign molecules during the synthesis. For example, X-ray diffraction (XRD) can be used to describe structural changes during the encapsulation process via XRD peak shifts and shape changes.[20] Nuclear magnetic resonance using ^{29}Si as a probe can be used to identify the silica network structure using the different peaks that are obtained during analysis; these peaks are related to the number of siloxane groups that each atom of Si can form.[21] Transmission electronic microscopy, N_2 adsorption, and small angle X-ray scattering were used to estimate pore size, surface area, and pore volume; these data were used to analyze the encapsulation time and content.[22] Rheological studies can be used to determine different structures on the silica, due to the presence of biological and bio-hybrid systems as diatoms with shear stress oscillatory measurements.[23] In addition, the pore volume and surface area changes due to the synthetic conditions can be observed using N_2 adsorption (the Brunauer, Emmett, and Teller method, commonly know as BET) and may hint at the material response observed during drug release.[24]

In FT-IR, the literature reports that the maximum centers and relative intensities of the longitudinal optic (LO) and

Received 30 May 2012; accepted 30 November 2012.
* Author to whom correspondence should be sent. E-mail: jhzds@iq.ufrgs.br.
DOI: 10.1366/12-06748

0003-7028/13/6704-0441/0

transversal optic (TO) modes of Si–O–Si asymmetric stretching are shifted with the introduction of chemical groups or organic molecules in the silica network.[14] When this band (Si–O–Si) is a fingerprint for silica, a complete analysis of its components can be conducted, including the deconvolution of the LO and TO modes and their relative contributions to the main siloxane ring unit [the four-membered ring $(SiO)_4$ and six-membered ring $(SiO)_6$, as illustrated in Scheme 1]. The band is composed of four basic elements, including the longitudinal components for the six-membered rings (LO_6) and the four-membered rings (LO_4) and the transversal components for the six-membered rings (TO_6) and the four-membered ring (TO_4).

Generally, samples with a higher content of chemical groups or organic molecules are more likely to show a six-membered ring formation, as these samples are less stressed, thereby allowing a better accommodation of the nonreactive organic groups. Furthermore, there is a correlation between the formation of six-membered rings and an increase in the relative degree of crystallinity, as well as with the long-range organization in hybrid silica materials that is normally observed with an increase in the degree of matrix alkylation.[25] The formation of $(SiO)_6$ can be tracked by the increasing contributions and a reduction in the LO_6 and TO_6 modes as shown through band deconvolution. Note a maximum band shift of these contributions may occur, as the LO mode is notably sensitive to network modifications, and the TO mode is not. This phenomenon may be observed as a result of the increase in content of organic groups within the silica network; these organic groups are responsible for the decrease of long-range Coulombic interactions. These decreased interactions, in turn, create the LO/TO separation.[14]

Herein, we use FT-IR and Raman spectroscopies as tools to obtain information about the interaction between pH indicators with the matrix and the indicator performance, in terms of response time and color change, when encapsulated within silica by the three sol-gel routes presented. We expect that additional information can be extracted by the analysis of the matrix and may provide some indirect clues about the effect of the presence of such pH indicators within the silica network. The investigated pH indicators are alizarin red (AL), brilliant yellow (BY), and acridine (AC), and the sol-gel routes we use include the hydrolytic acid-catalyzed route (AR), hydrolytic base-catalyzed route (BR) and a non-hydrolytic route (NHR). The indicators were chosen due to their different molecule volumes, their interactions with different functional groups (–OH, azo, and pyridine), and their equivalent point near pH 7.0. The different routes were chosen to evaluate different material properties associated with the formed matrices. In addition, we used infrared spectroscopy to evaluate the silica network structure in relation to the three different sol-gel routes (AR, BR, and NHR) and the three different pH indicators (AL, BY, and AC) used to prepare the acid–base sensor materials.

MATERIALS AND METHODS

Materials. Tetraethoxysilane [$Si(OCH_2CH_3)_4$, TEOS, Merck, >98% purity] and silicon tetrachloride ($SiCl_4$, Sigma-Aldrich, 99%) were used as received. The acid–base indicators AL (97%), BY (70%), and AC (97%) were obtained from Sigma-Aldrich. Hydrochloric acid (HCl, Nuclear, 38%), ammonium hydroxide (NH_4OH, Nuclear, 29%), and iron(III) chloride ($FeCl_3$, Merck, 98%,) were used as catalysts.

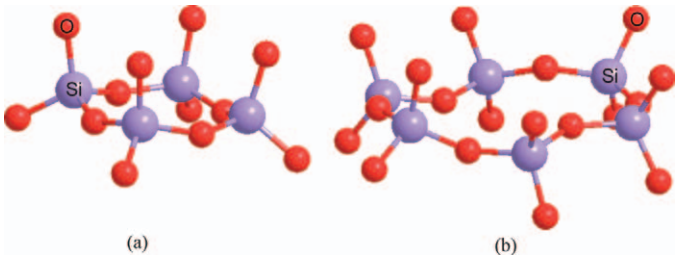

SCHEME 1. Two of the most common cyclical arrangements of SiO_4 structural units in xerogels. (**a**) Four-membered siloxane ring, $(SiO)_4$. (**b**) Six-membered siloxane ring, $(SiO)_6$.[14]

Sensor Materials Synthesis Using the Sol-Gel Process. Three different routes were used to prepare the sensor materials using the sol-gel process with TEOS as the raw material. The acid–base indicators were AL, BY, and AC, and the three routes were AR, BR, and NHR. The AR used HCl (1 : 20, HCl:TEOS ratio) as a catalyst, and the BR used NH_4OH (1 : 1, NH_4OH : TEOS ratio) as a catalyst. The NHR used TEOS and $SiCl_4$ and was catalyzed by $FeCl_3$ (0.5 wt% of the final product weight). The quantity of the acid–base indicator used was 0.1 mol% of the total amount of the alkoxide groups.

The sensor materials (powder) obtained by the acid- and base-catalyzed routes were prepared using aqueous or ethanolic solutions of the acid–base indicators, respectively, to which the catalyst and TEOS were added while stirring at room temperature. The resulting solution was stirred until gelation occurred (approximately 4 h for the AR) or until precipitation followed by one additional hour of stirring (total of 1 h 15 min for BR). For the NHR, all procedures were performed under an inert atmosphere. First, the catalyst and the indicator were combined, and TEOS and $SiCl_4$ were subsequently added. The solution was stirred at 80 °C until gelation occurred (approximately 2 h). All solids were milled, washed with water and ethanol to remove loosely entrapped indicators, and dried at 110 °C for 12 h. All of these procedures are described in detail elsewhere.[5] For each route, a corresponding blank (silica without the encapsulation of the pH indicator AL, BY, and AC) was prepared. The encapsulated content was quantified by UV-Vis spectroscopy with a diffuse reflectance accessory as described elsewhere.[26] Textural characteristics of the resulting materials is reported elsewhere.[5]

Hereafter, the resulting sensor materials are labeled according to the indicator and the sol-gel route. For example, ALNHR refers to the sensor materials prepared through a NHR containing AL as the indicator.

Fourier-Transformed Infrared Spectroscopy. The FT-IR spectra of the sensor materials and the silica were obtained using a FTIR-8300 instrument (Shimadzu) in the absorbance mode co-adding 32 scans with 4 cm^{-1} resolution. The spectra were measured in the range of 4000–500 cm^{-1}. Samples were pressed into tablets of approximately 1 mm in thickness and 5 mm in diameter. A dilution of approximately 10% was prepared in dried potassium bromide (KBr). Band deconvolution was performed using Gaussian curves in the region from 1350 to 1000 cm^{-1}.

Raman Spectroscopy. Measurements were performed at room temperature using an inVia Raman spectrometer (Renishaw) equipped with a near-infrared diode laser (785 nm), a charge-coupled detector, a 1200 lines mm^{-1} diffraction grating, and an edge filter. The samples were mounted on an

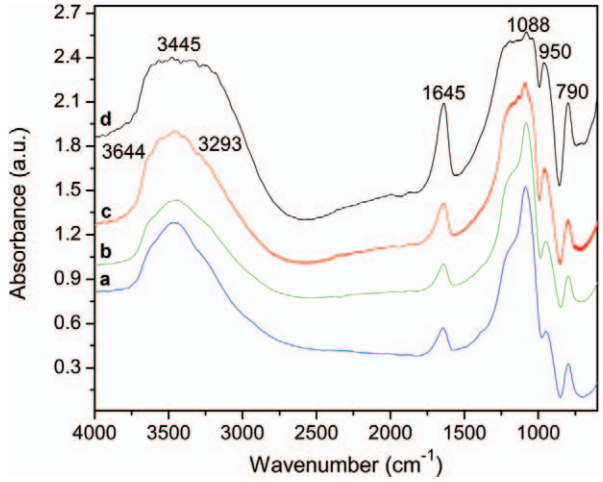

FIG. 1. FT-IR spectra for the sensors and silica, as obtained by an acidic route. (**a**) SiO_2. (**b**) ARBY. (**c**) ARAL. (**d**) ARAC.

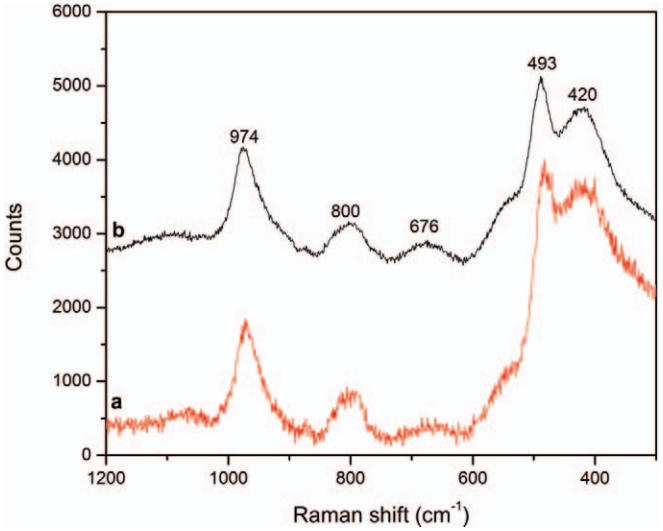

FIG. 2. Raman spectra for the sensors with alizarin red. (**a**) BRAL. (**b**) ARAL.

XYZ manual stage of a microscope (Leica), and the laser beam was focused onto the samples through a 20× long-working distance objective. The spectra were recorded using laser power adjusted between 15 and 300 mW and a slit width of 50 nm. Several scans were collected to improve the signal-to-noise ratio. The acquisition time was varied from sample to sample in the range from 10 to 60 s. The Raman spectrometer was calibrated before acquiring measurements by exciting a Si wafer placed under the microscope and performing an automatic offset correction. Data acquisition and analysis were accomplished using WiRETM software. The wavenumbers are estimated to be accurate to at least ± 1 cm^{-1}.

Small-Angle X-ray Scattering (SAXS). SAXS experiments were carried out on the D2A and D11A beamlines at the Brazilian Synchrotron Light Laboratory (LNLS, Campinas, Brazil) using a wavelength $\lambda = 1.488$ nm. The X-ray beam was monochromatized by a Si monochromator and collimated by a set of slits defining pinhole geometry. The incident beam was detected at two different sample-to-detector distances (1549.8 and 2245.7 mm) to increase the scattering vector (q) [$q = (4\pi/\lambda)\sin\theta$; 2θ = scattering angle) range. The dried samples were sandwiched between two pieces of Kapton® foil, and the collimated X-ray beam was passed through a chamber containing the stainless steel sample holder. All measurements were performed at room temperature. Transmission, dark current, and Kapton foil corrections were performed on the two-dimensional image before further data processing. The isotropic scattering patterns were radially averaged. SAXS data analysis was performed using the Irena evaluation routine[27] implemented in the IGOR Pro Software (Wavemetrics, Lake Oswego, OR).[28] A multilevel unified fit was used to describe one or two levels of structural organization evident in the scattering data[29,30] as described elsewhere.[5]

RESULTS AND DISCUSSION

For the sensor materials structure analyses, FT-IR and Raman spectroscopy were used. Initially, these techniques were used to evaluate the structure of the pH indicators within the silica matrix. Figure 1 illustrates the spectra obtained for the samples prepared by AR; this route provided the highest encapsulated indicator content. Similar spectra were observed for the other samples. The primary bands obtained were the $\nu_{(O-H)}$ vibrations of silanol groups (Si–OH) and adsorbed water (H_2O) centered approximately 3445 cm^{-1}; the δ_{H-O-H} of H_2O at 1645 cm^{-1}; the strong band with the maximum at 1088 cm^{-1} due to $\nu_{as(Si-O(-Si))}$ of the siloxanes' vibration of the silica network; the $\nu_{(Si-O)}$ vibration associated with dangling oxygen atoms on the silica structure at 950 cm^{-1}; and the band approximately 790 cm^{-1} corresponding to the bending vibrations of Si–O–Si network.[31] The shoulders of the band centered at 3445 cm^{-1} are also due to vibrations of the O–H groups. The shoulder at approximately 3293 cm^{-1} is probably due to the O–H(. . .O) groups, where OH groups are interacting by hydrogen bonds; and the shoulder at approximately 3644 cm^{-1} is characteristic of primary alcohols. This observation could be due to ethanol residue and to Si–OH absorption, such as that from alcohols.[31] No band was detected belonging to functional groups associated with indicator molecules.

In Fig. 2, the Raman spectra of ARAL and BRAL are shown. The sample correspondent to NHRAL was decomposed by the laser shot during analysis. The strongest band centered at 974 cm^{-1} is assigned to Si–O(H) stretching. Numerous structural models have been proposed for the band at 493 cm^{-1} and the shoulder at 610 cm^{-1}; these signals mainly arise from defects, such as broken Si–O bonds or the breathing modes of planar rings on the order of $n = 4$ (fourfold) or 3 (threefold), where n is the number of (SiO) groups in a ring.[32] The bending modes (O–Si–O, Si–O–Si) are omnipresent, and the torsions also are omnipresent. Stretching contributions from 650 to 900 cm^{-1} and the peak at 420 cm^{-1} are due to O–Si–O.[33,34] As with FT-IR, no band could be detected resulting from indicator molecules, but the silica structure could be evaluated.

Attempts to investigate the structure of the encapsulated pH indicators failed using both Raman and FT-IR spectroscopies because the presence of the indicators could not be detected (Figs. 1 and 2). Vibrational bands associated with these indicators were not detected. However, the presence of such molecules could be confirmed by UV-diffuse reflectance spectroscopy.[5] The absence of an indicator peak could be explained by the low concentration of the pH indicators (approximately 0.13–15 μmol g^{-1} silica), and in FT-IR, the samples were further diluted in KBr. However, in the Raman

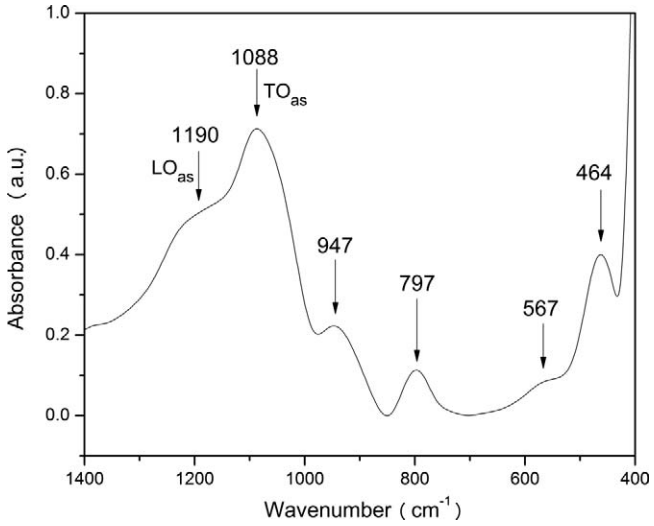

FIG. 3. Characteristic bands of Si–O–Si vibrations in bare silica, as obtained by an acidic route.

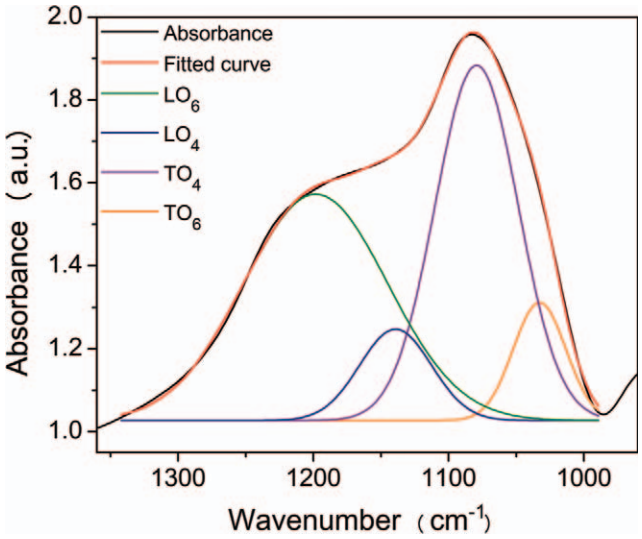

FIG. 4. Band deconvolution to asymmetric stretching $\nu_{(Si–O(–Si))}$ bond in ARBY FT-IR spectra.

analysis, the indicators were not detected, and this technique does not dilute the samples for analysis.

Although none of the samples shows spectra with peaks associated with pH indicators, FT-IR is useful for interpreting the silica structure that results from the presence of the encapsulated indicator. Vibrational spectra have been used to obtain information about the silica network, such as the Si–O–Si bond stress (related to normal values of inter-tetrahedric angle and bond length), porosity, and film thickness. [19,35] Furthermore, the Si–O–Si bands that have been taken as a fingerprint for silica[19,35] can provide information about the primary cyclic arrangements of structural SiO_4 units in xerogels, and this information, in turn, can be related to the crystallinity and hydrophilicity–lipophilicity balance.[14,18] Thus, the influence of the pH indicator on the silica network can be explored indirectly using FT-IR. Figure 3 shows the region over which these bands are observed, a region that corresponds to Si–O–Si bond and its vibration modes to the AR silica (as an example). The other samples presented exactly the same bands with different intensities and small wavenumber shifts.

In Fig. 3, the TO and LO optic modes of Si–O–Si and the bands centered at 567 and 947 cm^{-1} can be observed. The latter band corresponds to Si–O^- group stretching, and the former band is attributed to the rocking mode of the same species. The most intense band at 1088 cm^{-1} occurs due to the asymmetric stretching of sequential Si–O–Si groups in the TO mode, and its shoulder at approximately 1190 cm^{-1} has been related as the LO element of the same vibration.[19,36] Other TO modes are observed at 797 cm^{-1}, corresponding to bending vibrations, and at 464 cm^{-1}, corresponding to rocking vibrations. The bending vibrations are those where O atom vibrations occur along the plane and along the angle bisector formed by Si–O–Si, areas shown to be almost impervious to structural changes. However, the rocking mode of Si–O is where oxygen moves out of the plane of Si–O–Si.[36]

Due to the potential relevant information given by FT-IR and the deconvolution of the fingerprint band of silica, the present systems were evaluated in terms of the LO and TO modes for four- and six-membered rings. This procedure was an attempt to understand the silica structure as a function of the pH indicators present. The bands corresponding to the Si–O–Si bond from 1300 to 1000 cm^{-1} were deconvoluted using four Gaussian curves, with one band being used for each cited mode.[18] As an example, Fig. 4 shows the band corresponding to an ARBY sample spectra deconvoluted into four components, and the $(SiO)_6$ contents were calculated according to the following equation:

$$\%(\mathrm{SiO})_6 = 100 \times \left[\frac{A(\mathrm{LO}_6) + A(\mathrm{TO}_6)}{A(\mathrm{LO}_6) + A(\mathrm{LO}_4) + A(\mathrm{TO}_4) + A(\mathrm{TO}_6)}\right]$$

Figure 4 shows that a good fit could be obtained for the curve corresponding to the original spectra using deconvolution in four components. This procedure was repeated for all samples synthesized by the three different routes. The results to the maximum peak center wavenumber, relative area, variance, and $(SiO)_6$ percentage are shown in Table I. The $(SiO)_6$ percentage ranged from 50% to 60%, with the exception of the sample NHRAC that has a higher value. However, wavenumber shifts corresponding to the increase in these percentages were not verified, as shown by Fidalgo et al.[14]

Because the percentage of $(SiO)_6$ may reflect the presence of organic groups or molecules encapsulated within the silica network, Fig. 5 correlates the $(SiO)_6$ values with the encapsulated indicator content. For the AR sensor materials, we observed that there is a correlation between these two parameters [indicator content and $(SiO)_6$ percentage] for the samples in which indicators were added during the synthesis. However, the sample that does not contain the indicator ($ARSiO_2$) has an anomalous behavior that extends to the S/V ratio and the radius of gyration (R_g) for the primary particles measured by SAXS (Table II). Considering the absence of pH indicators, the pores of this material should be empty. This ratio may be higher relative to the samples that had pH indicators within the matrix. This finding suggests that the reactions of hydrolysis and condensation were influenced by the presence of the indicator, and this influence could explain the anomalous behavior. A comparison with SAXS data (from Ref. 5) for the samples with pH indicators (for AR) is also available. It was possible to observe a decrease in the R_g and S/

TABLE I. Areas of each contribution, as obtained by deconvolution of the band between 1300 and 1000 cm^{-1} and the $(SiO)_6$ percentage for each sample.

Sample	LO_6	LO_4	TO_4	TO_6	r^2	% $(SiO)_6$[a]
	Band center (cm^{-1}); area (a.u.)[b]					
$RASiO_2$	1195; 46.40	1156; 1.54	1084; 38.07	1034; 8.56	0.9998_1	58.11
RAVA	1195; 76.37	1111; 36.14	1070; 35.35	1037; 8.42	0.9987_6	54.26
RAAB	1198; 72.77	1139; 14.67	1079; 65.95	1033; 13.92	0.9995_5	51.81
RAAC	1192; 20.23	1106; 6.31	1074; 8.74	1042; 2.17	0.9970_2	59.81
$RBSiO_2$	1199; 116.75	1167; 4.92	1116; 107.84	1060; 94.76	0.9998_8	65.23
RBVA	1202; 110.23	1155; 23.29	1099; 125.43	1052; 34.23	0.9992_3	49.27
RBAB	1189; 24.64	1154; 83.06	1097; 6.04	1050; 74.25	0.9986_1	52.60
RBAC	1192; 79.27	1147; 12.09	1099; 58.99	1055; 38.24	0.9989_5	62.31
$RNHSiO_2$	1193; 43.93	1152; 3.73	1088; 47.51	1039; 10.42	0.9995_1	51.47
RNHVA	1189; 57.10	1141; 4.04	1080; 42.69	1036; 9.37	0.9988_9	58.72
RNHAB	1185; 43.55	1146; 2.17	1078; 37.79	1029; 9.62	0.9992_4	57.09
RNHAC	1219; 15.85	1142; 23.12	1093; 3.04	1050; 46.53	0.9998_1	70.45

[a] In a confidence level of 95% ($p = 0.05$), the confidence limits were from 53% to 62%.
[b] Arbitrary units.

V values that corresponds with an increasing of the $(SiO)_6$ percentage and pH indicator content. Because the primary particles were on the order of 1 nm, they were probably composed of SiO_4 units that can contract their volume to form $(SiO)_6$ rings and provide room to accommodate the pH molecules in the pores. The S/V decrease was also due to the pH indicator presence, and because these molecules tended to lodge themselves in the pores, the ratio decreased during filling, which was higher for higher pH indicator contents.

For the BR, no correlation was established, but it is important to note that the encapsulated content for this route is notably small—approaching zero. In addition, it was not possible to establish relationships with SAXS because the parameters could not be fitted for all samples. Similar behavior was observed in the NHR. Nevertheless, taking into account the $(SiO)_6$ percentage, the NHR seems to be the route most influenced by the pH indicators, within the silica network, as they exhibit the highest change in the $(SiO)_6$ percentage as a function of the encapsulated indicator content. This behavior could be explained by the rearrangement of the $(SiO)_4$ ring units in a structure with less tension [$(SiO)_6$] that can easily accommodate the organic species in the tridimensional network. It is worth noting that by changing the sol-gel route, the rate between hydrolysis and condensation reactions may differ as a function of the pH medium. This finding could explain the behavior of the BR sensor material. Under basic conditions, the condensation reactions of the silanol groups are strongly accelerated, and the particles are formed overly rapidly. Thus, the probability of rearrangement as a function of the presence of other molecules (in the present case, pH indicators) during the synthesis decreases because the tridimensional network is rapidly formed. When these reactions are slower, such as with reactions in acid pH, the network can be influenced more by the addition of molecules to be encapsulated.[37] However, the average $(SiO)_6$ percentage values for each route do not show large differences as a function of the route itself. A difference of two percentage points was found for each route in the following sequence: AR less than BR less than NHR.

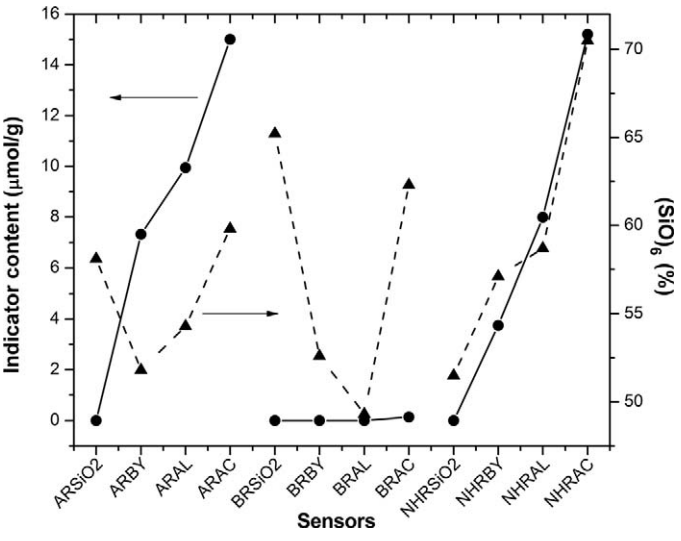

FIG. 5. Comparison of percentage of $(SiO)_6$ (▲) and encapsulated indicator content (•) in each sample.

This behavior indicates that the relationships between the organic content and the $(SiO)_6$ percentages described in the literature[14] can be applied to an encapsulation process, where organic molecules, in this case, are present within the silica network. These results may be important to interpret materials behavior with respect to interactions between the analyte and the response time for sensor materials as a function of the silica network structure. Note that the encapsulated contents of the indicators are minute (micromoles per gram) and that this amount may affect the quantification of structural deviations, as well as the anomalous behaviors and the small changes observed. In the sensor materials preparation, the response time to detect an analyte is an important feature. Normally, higher specific areas and matrices with higher access to the analyte permeation may reduce the response time, thereby improving the sensor performance.[5] Due to the importance of this feature, an investigation between the matrix structure and the response time is relevant; however, no relationship between the $(SiO)_6$ percentage and the sensor response time can be reported because there was no correlation with the sensor response time.[5] Thus, analyte penetration through the silica matrix did not seem to be determined by the dimension of the rings. So, bigger siloxane rings did not favor shorter response times, since the permeation is easier through bigger rings. This observation may indicate that the analyte can access receptor elements through the spaces external to the siloxane rings and not through the siloxane rings themselves.

TABLE II. S/V ratios and R_g[5] values for sensor materials and bare silica, as measured by SAXS.

	AR		BR		NHR	
	S/V, cm^{-1}	R_g, nm	S/V, cm^{-1}	R_g, nm	S/V, cm^{-1}	R_g, nm
AL	5015	1.2	3677	1.4	—	—
BY	7082	1.4	—	—	—	—
AC	2032	1.1	3013	2.0	82	—
Bare SiO_2	3900	1.1	80	—	—	—

The sensors were tested in ammonia gas-sensing and aqueous solutions, including real samples from a galvanic industry. The colors and results have been reported previously.[38] Between pH 2.0 and 8.0, the color did not change, hindering the accurate measurement in this range. The sensors also were tested for reusing by their recuperation after contact with ammonia gas or with solution having up to pH 14.0. After the contact, the materials were then heated for reusing. All sensors could be reused and remained active after five cycles. The life times were longer than two years, since the materials remain active. The sensor materials were tested in real samples (galvanic industry effluent) as reported previously.[38]

CONCLUSION

According to this study, the best route for preparing sensor materials is the hydrolytic-acid-catalyzed route. The present study shows that the pH indicators in the 0.13–15.7 μmol g^{-1} range cannot be detected by FT-IR or Raman spectroscopy. It was possible to identify only the bands corresponding to silica and the associated network vibrational modes. These techniques were successfully used to evaluate the silica network structure in relation to the sol-gel route used, the nature of the indicator, and the indicator content in each sensor material using a peak deconvolution corresponding to the TO and LO modes of the Si–O–Si asymmetric vibration. For the acidic and non-hydrolytic routes, it was possible to extract a positive correlation between the pH indicator content and the increase of $(SiO)_6$ percentage, thereby indicating a rearrangement of the structure to accommodate the indicator molecules. For the basic route, this relationship was not observed. Nevertheless, the indicator contents were notably low. No relationship between the $(SiO)_6$ percentage and the response time could be established in spite of less dense networks, with bigger rings, might render easier the analyte penetration. This behavior may indicate that the analyte probably accessed receptor elements through the passages between the siloxane rings and not through the siloxane rings themselves. Further research is necessary for developing sensor films prepared by techniques such as dip- or spin coating.

ACKNOWLEDGMENTS

This project was partially financed by the Conselho Nacional de Desenvolvimento Científico e Tecnológico (CNPq) and Fundação de Apoio da Universidade Federal do Rio Grande do Sul-Braskem. Larissa B. Capeletti thanks CNPq for the grant, and all authors thank LNLS (project D11A-SAXS1-8691) for measurements in the SAXS beamline.

1. J. Chen, J. X. "SnO(2)-Based R134a Gas Sensor: Sensing Materials Preparation, Gas Response and Sensing Mechanism". Sens. Actuators B Chem. 2011. 157(2): 494-499.
2. T.V. Duncan. "Applications of Nanotechnology in Food Packaging and Food Safety: Barrier Materials, Antimicrobials and Sensors". J. Colloid Interface Sci. 2011. 363(1): 1-24.
3. J. Huang, C.-A. Tao, Q. An, C. Lin, X. Li, D. Xu, Y. Wu, X. Li, D. Shen, G. Li. "Visual Indication of Environmental Humidity by Using Poly(Ionic Liquid) Photonic Crystals". Chem. Commun. 2010. 46(23): 4103-4105.
4. T. Kuila, S. Bose, P. Khanra, A.K. Mishra, N.H. Kim, J.H. Lee. "Recent Advances in Graphene-Based Biosensors". Biosens. Bioelectron. 2011. 26(12): 4637-4648.
5. R. Buntem, A. Intasiri, W. Lueangchaichaweng. "Facile Synthesis of Silica Monolith Doped with Meso-Tetra(p-Carboxyphenyl)-Porphyrin as a Novel Metal Ion Sensor". J. Colloid Interface Sci. 2010. 347(1): 8-14.
6. P.C.A. Jeronimo, A.N. Araujo, M. Montenegro. "Optical Sensors and Biosensors Based on Sol-Gel Films". Talanta. 2007. 72(1): 13-27.
7. A. Walcarius, M.M. Collinson. "Analytical Chemistry with Silica Sol-Gels: Traditional Routes to New Materials for Chemical Analysis". Annu. Rev. Anal. Chem. 2009. 2: 121-143.
8. L.B. Capeletti, F.L. Bertotto, J.H.Z. Dos Santos, E. Moncada, M.B. Cardoso. "The Effect of the Sol-Gel Route on the Characteristics of Acid-Base Sensors". Sens. Actuators B Chem. 2010. 151(1): 169-176.
9. X.Q. Li, J.J. Yuan, H.A. Liu, L. Jiang, S.Q. Sun, S.Y. Cheng. "Microgel-Silica Hybrid Particles: Strategies for Tunable Nanostructure, Composition, Surface Property and Porphyrin Functionalization". J. Colloid Interface Sci. 2010. 348(2): 408-415.
10. L.T. Arenas, D.S.F. Gay, C.C. Moro, S.L.P. Dias, D.S. Azambuja, T.M.H. Costa, E.V. Benvenutti, Y. Gushikem. "Brilliant Yellow Dye Immobilized on Silica and Silica/Titania Based Hybrid Xerogels Containing Bridged Positively Charged 1,4-Diazoniabicyclo[2.2.2]Octane: Preparation, Characterization and Electrochemical Properties Study". Microporous Mesoporous Mater. 2008. 112(1-3): 273-283.
11. I. Negron-Encarnacion, R. Arce, M. Jimenez. "Characterization of Acridine Species Adsorbed on $(NH_4)_2SO_4$, SiO_2, Al_2O_3, and MgO by Steady-State and Time-Resolved Fluorescence and Diffuse Reflectance Techniques". J. Phys. Chem. A. 2005. 109(5): 787-797.
12. R. Brambilla, J. Poisson, C. Radtke, M.S.L. Miranda, M.B. Cardoso, I.S. Butler, J.H.Z. dos Santos. "Sol-Gel Preparation of Aminopropyl-Silica-Magnesia Hybrid Materials". J. Sol-Gel Sci. Technol. 2011. 59(1): 135-144.
13. A. Fidalgo, R. Ciriminna, L.M. Ilharco, M. Pagliaro. "Role of the Alkyl-Alkoxide Precursor on the Structure and Catalytic Properties of Hybrid Sol-Gel Catalysts". Chem. Mater. 2005. 17(26): 6686-6694.
14. F. Adam, A. Iqbal. "Silica Supported Amorphous Molybdenum Catalysts Prepared via Sol-Gel Method and Its Catalytic Activity". Microporous Mesoporous Mater. 2011. 141(1-3): 119-127.
15. N. Bellec, F. Lerouge, O. Jeannin, G. Cerveau, R.J.P. Corriu, D. Lorcy. "Auto-Organization Modulation of Tetrasubstituted Tetrathiafulvalenes (TTF) in Silica Based Hybrid Materials". J. Organomet. Chem. 2006. 691(26): 5774-5781.
16. L.B. Capeletti, C. Radtke, J.H.Z. Dos Santos, E. Moncada, Z.N. Da Rocha, I.M. Pepe. "On the Interaction of Encapsulated pH Indicator Species Within a Silica Matrix Produced by Three Sol-Gel Routes". Colloids Surf. A. Physicochem. Eng. Asp. 2011. 392(1): 256-263.
17. A. Fidalgo, L.M. Ilharco. "Chemical Tailoring of Porous Silica Xerogels: Local Structure by Vibrational Spectroscopy". Chem. Eur. J. 2004. 10(2): 392-398.
18. R.M. Almeida, T.A. Guiton, C.G. Pantano. "Detection of LO Mode in V-SiO_2 by Infrared Diffuse Reflectance Spectroscopy". J. Non. Cryst. Solids. 1990. 119(2): 238-241.
19. I.M. Arafa, M.M. Fares, A.S. Barham. "Sol-Gel Preparation and Properties of Interpenetrating, Encapsulating and Blend Silica-Based Urea-Formaldehyde Hybrid Composite Materials". Eur. Polym. J. 2004. 40(7): 1477-1487.
20. A. Pierre, J. Bonnet, A. Vekris, J. Portier. "Encapsulation of Deoxy-

ribonucleic Acid Molecules in Silica and Hybrid Organic-Silica Gels". J. Mater. Sci. Mater. Med. 2001. 12(1): 51-55.
21. H. Gustafsson, C. Thorn, K. Holmberg. "A Comparison Of Lipase and Trypsin Encapsulated in Mesoporous Materials with Varying Pore Sizes and pH Conditions". Colloids Surf. B. Biointerfaces. 2011. 87(2): 464-471.
22. C. Gautier, A. Ponton, J. Livage, P.J. Lopez, T. Coradin. "Rheological Studies Of Diatom Encapsulation in Silica Gel". J. Sol-Gel Sci. Technol. 2009. 50(2): 164-169.
23. P. Prawingwong, C. Chaiya, P. Reubroycharoen, C. Samart. "Utilization of Rice Husk Ash in Controlled Releasing Application". J. Met. Mater. Min. 2009. 19: 5.
24. S.L.B. Lana, A.B. Seddon. "X-ray Diffraction Studies of Sol-Gel Derived ORMOSILs Based on Combinations of Tetramethoxysilane and Trimethoxysilane". J. Sol-Gel Sci. Technol. 1998. 13(1-3): 461-466.
25. L.B. Capeletti, J.H.Z. dos Santos, E. Moncada. "Quantification of Indicator Content in Silica-Based pH Solid Sensors by Diffuse Reflectance Spectroscopy". Anal. Methods. 2011. 3(10): 2416-2420.
26. J. Ilavsky, P.R. Jemian. "Irena: Tool Suite for Modeling and Analysis of Small-Angle Scattering". J. Appl. Crystallogr. 2009. 42: 347-353.
27. S.R. Kline. "Reduction and Analysis of SANS and USANS Data Using IGOR Pro". J. Appl. Crystallogr. 2006. 39: 895-900.
28. G. Beaucage. "Approximations leading to a unified exponential power-law approach to small-angle scattering". J. Appl. Crystallogr. 1995. 28: 717-728.
29. G. Beaucage. "Small-Angle Scattering from Polymeric Mass Fractals of Arbitrary Mass-Fractal Dimension". J. Appl. Crystallogr. 1996. 29: 134-146.
30. N.B. Colthup, L.H. Daly, S.E. Wiberley. Introduction to Infrared and Raman Spectroscopy. San Diego, CA: Academic Press, 1990. 3rd ed.
31. B.A. Morrow, D.T. Molapo. "Infrared Studies of Chemically Modified Silica". In: H.E. Bergna, W.O. Roberts, editors. Colloidal Silica: Fundamentals and Applications. Boca Raton, FL: CRC Press, 2005. Pp. 287-310.
32. S.W. da Silva, R.C. Pedroza, P.P.C. Sartoratto, D.R. Rezende, A.V.D. Neto, M.A.G. Soler, P.C. Morais. "Raman Spectroscopy of Cobalt Ferrite Nanocomposite in Silica Matrix Prepared by Sol-Gel Method". J. Non. Cryst. Solids. 2006. 352(9-20): 1602-1606.
33. M. Dracinsky, L. Benda, P. Bour. "Ab Initio Modeling of Fused Silica, Crystal Quartz, and Water Raman Spectra". Chem. Phys. Lett. 2011. 512(1-3): 54-59.
34. R.M. Almeida. "Handbook of Sol-Gel Science and Technology: Processing, Characterization and Applications". New York: Kluwer Academic Press, 2004.
35. I. Montero, L. Galan, O. Najmi, J.M. Albella. "Disorder-Induced Vibration-Mode Coupling in SiO_2-Films Observed Under Normal-Incidence Infrared Radiation". Phys. Rev. B. Condens Matter. 1994. 50(7): 4881-4884.
36. C.J. Brinker. "Hydrolysis and Condensation Silicates—Effects on Structure". J. Non. Cryst. Solids. 1988. 100(1-3): 31-50.
37. L. Capeletti, J.H.Z. Dos Santos, E. Moncada. "Dual-Target Sensors: the Effect of the Encapsulation Route on pH Measurements and Ammonia Monitoring". J. Sol-Gel Sci. Technol. 2012. 64(1): 209-218.